Mon. Not. R. astr. Soc. (1975) **171**, 87–102.

CENTRAL GRAVITATIONAL REDSHIFTS FROM STATIC MASSIVE OBJECTS

P. K. Das and J. V. Narlikar

Tata Institute of Fundamental Research, Homi Bhabha Road, Bombay 400 005, India

(Received 1974 November 8; in original form 1974 September 6)

SUMMARY

The possibility of obtaining high gravitational redshifts from static massive objects is investigated in an attempt towards finding a satisfactory explanation of the redshifts of the QSOs. Following Bondi's approach equilibrium configurations of the core and envelope type are discussed within the framework of general relativity. Gravitational redshifts from the centre of the core, from the core–envelope boundary and from the surface of the object are calculated in a variety of cases and their dependence on the equation of state is studied. In a possible application of these models to QSOs the emission is considered to arise from an optically thin central region surrounded by an exterior which lets through a fraction of the emitted light. The mass of such an object can be estimated from the emission line data, as discussed with the example of 3C 9.

1. INTRODUCTION

The interpretation of the spectacularly large redshifts of the quasi-stellar objects (QSOs) is one of the most critical problems in astronomy today. By now all the three conventional explanations of redshift, namely, cosmological, gravitational and Doppler have been tried and a fair assessment of the existing data (**1**) leaves strong doubts whether any one of these can represent the whole truth. In particular, the cosmological explanation, believed to be correct by majority of astronomers may not account for the entire redshift of a QSO, as some of the data on discrepant redshifts seems to suggest (**2**, **3**). It is possible to visualize a situation in which the total redshift z of a QSO is made up of the cosmological component $z_{\rm cos}$ and an intrinsic component $z_{\rm int}$ in the following way

$$(1+z) = (1+z_{\rm cos})(1+z_{\rm int}). \qquad (1)$$

In this paper we investigate models giving rise to large values of $z_{\rm int}$ through the phenomenon of the gravitational redshift.

As mentioned above, there are difficulties with the standard interpretation in which the gravitational redshift arises from the surface of a collapsed object. Greenstein & Schmidt (**4**) have pointed out the difficulty of accounting for strong emission into narrow spectral lines. Their calculations for Hβ emission from 3C 273 and 3C 48 seemed to rule out the possibility of these QSOs being highly collapsed stars in the Galaxy. Instead, their masses turn out to be at least as high as 10^8–$10^{10}\,M_\odot$ and their location just beyond our Galaxy, if not further. These values were considered implausible, and this idea was not carried further. A second difficulty came with the theoretical results obtained by Bondi (**5**) who demonstrated that even by stretching the equation of state to the limits permitted by

conventional physics, the surface redshift from a spherical mass in equilibrium cannot exceed the value 0·62. Therefore, unless we are willing to consider the QSOs as collapsing objects close to becoming black holes, very high values of z_{int} cannot be obtained for them. For example, the redshift 3·4 of the QSO OH 471 cannot be entirely its surface gravitational redshift if it is an object in equilibrium.

A model in which these difficulties might be avoided was suggested in 1967 by Hoyle & Fowler (**6**). This consists of a central gas cloud giving rise to the emission lines and the continuum surrounded by a large number of compact highly collapsed subunits and floating clouds of ions. The subunits provide a strong gravitational field causing the radiation from the centre to be redshifted. This redshift from the centre, z_c is greater than the redshift from the surface, z_s. Also the original Greenstein–Schmidt type calculation does not apply to this model, although a revised form of it can still be applicable.

Hoyle & Fowler (1967) pointed out that in the limiting case of the Schwarzschild interior solution, $z_s \to 2$ and $z_c \to \infty$. However, in this case the central pressure $p_c \to \infty$ while the energy density ρ stays finite and constant throughout the object. Clearly this is unrealistic. Instead, one can ask the following question: ' By taking the equation of state within the limits permitted by conventional physics, what are the maximum values of z_c for equilibrium configurations? ' In answering this question we shall adopt the approach and notation of Bondi (1964, referred to hereafter as I).

We will also investigate the plausibility of such models in terms of the emission line data. For this we give the modified form of Greenstein–Schmidt calculation applicable to central redshift models. The discussion of other questions, e.g. binding energy, stability etc. of such models which may place further restrictions on these models will be given in a subsequent paper.

2. EQUILIBRIUM CONFIGURATIONS À LA BONDI

Bondi's models are based on the following assumptions: (i) The system is spherically symmetric and static. (ii) Space time is everywhere regular and there is a point centre (taken as origin) to the spherical symmetry. (iii) Outside a finite region space is empty and is therefore described by the Schwarzschild metric. (iv) The material in the non-empty portion of space is hydrostatically supported by an isotropic pressure. (v) At the outer boundary of the body the pressure vanishes. (vi) Pressure and density are everywhere finite except in the well-defined case of a thin mass shell. We will adopt the same assumptions.

As in I, we will assume general relativity to hold and will take $c = 1$, $G = 1$ in the field equations which now become

$$R_{ik} - \tfrac{1}{2} g_{ik} R = -8\pi T_{ik}. \tag{2}$$

Here R_{ik} is the Ricci tensor, R the scalar curvature and T_{ik} the energy momentum tensor. In the empty region $T_{ik} = 0$ and the Schwarzschild line element is given by

$$ds^2 = \left(1 - \frac{2M}{r}\right) dt^2 - \left(1 - \frac{2M}{r}\right)^{-1} dr^2 - r^2(d\theta^2 + \sin^2\theta \, d\phi^2) \tag{3}$$

in terms of the standard Schwarzschild coordinates. We will assume the empty region to be given by $r > r_s$ and the non-empty region by $r \leqslant r_s$. In the latter region

$T_{ik} \neq 0$, and we have

$$T^{i}_{k} = \text{diag}(-p, -p, -p, \rho), \tag{4}$$

and the line element is given by

$$ds^2 = e^{\nu}\,dt^2 - e^{\lambda}\,dr^2 - r^2(d\theta^2 + \sin^2\theta\,d\phi^2). \tag{5}$$

with p, ρ, ν and λ as functions of r only.

The gravitational mass in the region $r \leqslant r_1 \leqslant r_s$ is defined by

$$m(r_1) = \int_0^{r_1} 4\pi r^2 \rho(r)\,dr, \tag{6}$$

with $m(r_s) = M$. It is convenient to introduce two new variables defined by

$$u = \frac{m(r)}{r}, \quad v = 4\pi r^2 p. \tag{7}$$

The field equations (2) are then equivalent to the following set of equations:

$$r\frac{dv}{dr} = 2\frac{(u+v)}{(1-2u)}, \tag{8}$$

$$S = r\frac{du}{dr} = \frac{H}{(1-2u)\left(\dfrac{dv}{du} - \alpha\right)}, \tag{9}$$

$$4\pi r^2\rho = u\frac{\left(\dfrac{dv}{du} - \beta\right)}{\left(\dfrac{dv}{du} - \alpha\right)}, \tag{10}$$

$$\frac{dp}{dr} = -\tfrac{1}{2}(\rho + p)\frac{dv}{dr}, \tag{11}$$

where

$$\alpha = -\frac{(u+v)}{(1-2u)}, \quad \beta = -\frac{v}{u}\frac{(2-5u-v)}{(1-2u)}, \quad H = 2v - (u^2 + 6uv + v^2). \tag{12}$$

Given the equation of state, i.e. a relation between p and ρ, these equations determine v as a function of u. At the centre of the object $u = 0$, $v = 0$ whereas at the surface $v = 0$, $u \neq 0$. We will label all surface values of various parameters by the subscript s and all the central values by the subscript c. As in I we consider the various properties of the interior solution on a u–v diagram shown in Fig. 1. The important properties discussed by Bondi are summarized below.

(i) The hyperbola $H = 0$ (see Fig. 1) divides the interior region into two parts: the core and the envelope. The core is specified by $H \geqslant 0$ and the envelope by $H < 0$. We shall denote the core–envelope boundary values of the various physical quantities by the subscript b.

(ii) Any equilibrium distribution under the specified assumptions is given by a curve in the (u, v) plane. In order that r is finite the curve must intersect the hyperbola $H = 0$ at such an angle that $dv/du = \alpha$ at the point of intersection. This is required by (9).

(iii) We shall assume throughout that $p > 0$, $\rho > 0$ which implies that $v > 0$, $u > 0$ and that dv/du does not lie in the range between α and β. This follows from (10).

(iv) As we move outwards from the centre, (9) imposes a further restriction on the slope of the u–v curve at any point P on it. Through P draw the parabola given by $dv/du = \alpha$ and consider the tangent l_p to it at P. Then if P lies in the region $H > 0$, the outward direction at P along the u–v curve must lie above l_p. If $H < 0$ the outward direction is below l_p.

In I, Bondi discussed various equations of state for core and envelope subject to the above restrictions. The highest surface redshift corresponding to a highly unphysical model with a zero density core and a thin mass shell envelope of infinite volume density but finite surface density, comes out to be 4·77 whereas the value $z_s = 0{\cdot}62$ quoted earlier and referred to often in literature corresponds to an

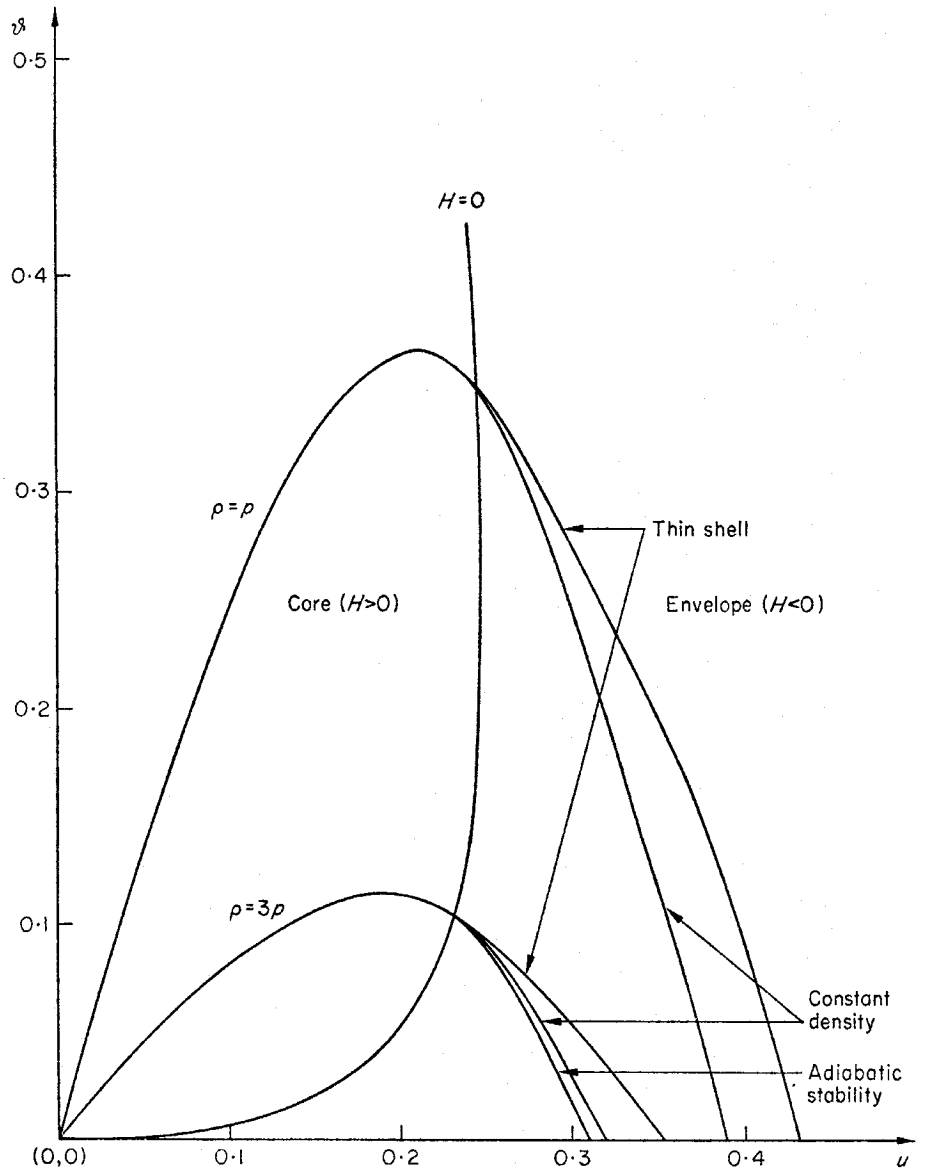

FIG. 1. *The u–v plane with curves representing isothermal cores* ($\rho = p$ *and* $\rho = 3p$) *and various envelopes.*

isothermal core ($\rho = 3p$) and an adiabatically stable envelope ($dp/d\rho = 1$: velocity of sound = velocity of light).

In the following we shall restrict our discussion to the two most stringent (and most physical) of the cases considered by Bondi, namely, (i) an isothermal core with an adiabatically stable envelope, and (ii) an isothermal core with a constant density envelope.

3. CENTRAL REDSHIFTS

A light wave emitted from the interior of the object, out to a great distance ($r \gg M$) away from it is redshifted by

$$z = e^{-\nu/2} - 1, \tag{13}$$

where ν is calculated at the point of emission. Thus we have

$$\begin{aligned} z_c &= e^{-\nu_c/2} - 1, \\ z_s &= e^{-\nu_s/2} - 1 = (1-2u_s)^{-1/2} - 1. \end{aligned} \tag{14}$$

To compute z_c, we need the equation for ν in terms of u and v. This is easily obtained from (8) and (9) in the form

$$\frac{dv}{du} = \frac{2(u+v)}{(1-2u)} \frac{1}{H} \left\{ (1-2u) \frac{dv}{du} + (u+v) \right\}. \tag{15}$$

Given v as a function of u, (15) can be integrated together with the boundary condition

$$\nu_s = \ln (1-2u_s). \tag{16}$$

In the extreme case of an empty core surrounded by a thin mass shell envelope we have the u–v curve given by

$$\begin{aligned} &\text{core:} \quad u = 0, \quad 0 \leqslant v < 2-\epsilon, \\ &\text{envelope:} \quad v = (3-\epsilon)\sqrt{1-2u} - (1-u), \\ &0 < u \leqslant u_s = 0{\cdot}485 - 0{\cdot}01\epsilon. \end{aligned} \tag{17}$$

It is easy to see that for this case

$$z_c = \frac{11{\cdot}55}{\epsilon} - 1. \tag{18}$$

Thus, as $z_s \to 4{\cdot}77$, $\epsilon \to 0$ and $z_c \to \infty$.

However, as mentioned earlier we shall consider more carefully the models with the core equation of state given by

$$p = k\rho, \tag{19}$$

and the envelope equation of state given by

$$\frac{dp}{d\rho} = \frac{1}{n}, \tag{20}$$

or by,

$$\frac{d\rho}{dr} = 0. \tag{21}$$

We may regard (19)–(21) as limiting forms of equations in which inequalities of the type $\leqslant$ are replaced by equalities. We will assume that k does not exceed unity. The restriction on n is given by

$$nk < 1. \tag{22}$$

This condition arises when we use (20) and require $\rho_s > 0$.

To determine the value of z_c in both these cases we use (11). In the case of (20), we have in the envelope

$$e^{\nu} = (1-2u_s)\left\{1+\frac{(n+1)\,p}{\rho_s}\right\}^{-2/(n+1)} \quad (r \geqslant r_b). \tag{23}$$

Similarly in the core we have

$$e^{\nu} = (1-2u_s)\left\{1+\frac{(n+1)\,p_b}{\rho_s}\right\}^{-2/(n+1)}\left(\frac{p_b}{p}\right)^{2k/(k+1)} \quad (r \leqslant r_b). \tag{24}$$

Hence we get the redshift from the core–envelope interface as given by z_b where

$$1+z_b = (1+z_s)\left(\frac{1+k}{1-nk}\right)^{1/(n+1)}. \tag{25}$$

The central redshift is given by

$$1+z_c = (1+z_s)\left(\frac{1+k}{1-nk}\right)^{1/(n+1)}\left(\frac{p_c}{p_b}\right)^{k/(k+1)}. \tag{26}$$

Thus if we have the solution $p = p(u)$, $v = v(u)$ available, we can calculate z_b and z_c with the help of (25) and (26) respectively.

The calculation in the case of (21) is also easy to perform. In this case in the envelope ρ = constant = ρ_b.
Hence ν is given by

$$e^{\nu} = (1-2u_s)\left(1+\frac{p}{\rho_b}\right)^{-2} \quad (r \geqslant r_b). \tag{27}$$

In the core, (19) continues to hold and we get

$$e^{\nu} = \frac{(1-2u_s)}{(1+k)^2}\left(\frac{p_b}{p}\right)^{2k/(k+1)} \quad (r \leqslant r_b). \tag{28}$$

In this case we have

$$(1+z_b) = (1+k)(1+z_s), \tag{29}$$

and

$$(1+z_c) = (1+k)(1+z_s)\left(\frac{p_c}{p_b}\right)^{k/(k+1)}. \tag{30}$$

In the first case, the numerical values of p_b/p_c etc. are available for the case $k^{-1} = 3$, $n = 1$ from I. Similarly the solutions are available from I in the second case for $k^{-1} = 1$ and $k^{-1} = 3$. Thus we can calculate the values of z_c, z_b and z_s in these cases. These values as well as the values for the extreme case of the thin mass shell are given in Table I. Note that the values of z_c and z_b are significantly greater than those of z_s in all cases.

TABLE I

Equation of state		Redshifts		
Core	Envelope	z_s	z_b	z_c
$\rho = 0$	Thin mass shell	4·77	4·77	∞
$\rho = p$	Thin mass shell	1·71	1·71	6·35
$\rho = p$	ρ = constant	1·13	3·26	10·56
$\rho = 3p$	Thin mass shell	0·84	0·84	2·09
$\rho = 3p$	ρ = constant	0·66	1·22	2·72
$\rho = 3p$	Adiabatic stability ($d\rho = dp$)	0·62	1·29	2·85

4. NUMERICAL COMPUTATIONS

We have investigated the first of the two cases in more detail, considering the core equation of state for a series of values of k and the envelope equation of state for a range of permitted n values for a specified k. Numerical solutions obtained with the help of a CDC-3600 computer are discussed below.

4.1 *Integration procedure*

The integration is done in the u–v plane from the origin outwards to the surface.

Core. The relevant equation (obtained from (10) and (19)) is

$$\frac{dv}{du} = \frac{-v(k+1)-u(5k+1)+2k}{(1-2u)(v-ku)}.v. \tag{31}$$

With the initial condition $dv/du = 3k$ at $u = 0$, $v = 0$ (31) was integrated till $H = 0$ was reached, for $k^{-1} = 2(1)$ 10, 25, 50, 100.

Envelope. For a given k, n can take values in the range $1 \leqslant n < k^{-1}$ ($n \geqslant 1$ ensures that sound velocity does not exceed light velocity). But as $n \to k^{-1}$ turning values of u tend to occur. So it was found convenient to use v as the independent variable.

The relevant equations are

$$\frac{dS}{dv} = \frac{n\{(u+v)^2+S(u+v)\}-(1-2u)(S+2u)}{S(u+v)-H}, \tag{32}$$

$$\frac{du}{dv} = \frac{S(1-2u)}{H-S(u+v)}. \tag{33}$$

With the initial conditions $u = u_b$, $S = S_b = v_b/k - u_b$ at $v = v_b$ these were integrated till $v = 0$ was reached. In addition the inequalities

$$\text{(i) } S+u>0; \quad \text{(ii) } \{S(u+v)-H\}>0 \tag{34}$$

were imposed to ensure positive density and to prevent a turning point of v, respectively.

The march of other related variables, e.g. p, ρ, r etc. was also determined throughout the model. The equations in fact calculate the dimensionless quantities p/p_c, ρ/ρ_c and

$$a = \sqrt{\frac{4\pi}{3}\rho_c}\, r. \tag{35}$$

TABLE II

The three values of redshifts for any pair (k^{-1}, n) are respectively z_a, z_b and z_c

Core $p = k\rho$ k^{-1}	Envelope $d\rho = n\,dp$ n 1	2	3	4	5	6	7	8	9
	0·75								
2	2·02								
	4·90								
	0·62	0·55							
3	1·29	1·47							
	2·83	3·12							
	0·52	0·49	0·44						
4	0·96	1·03	1·16						
	1·99	2·08	2·28						
	0·45	0·43	0·41	0·37					
5	0·77	0·80	0·85	0·96					
	1·54	1·58	1·65	1·80					
	0·39	0·38	0·37	0·35	0·31				
6	0·65	0·66	0·69	0·73	0·82				
	1·25	1·28	1·31	1·37	1·48				
	0·35	0·34	0·33	0·32	0·30	0·27			
7	0·56	0·57	0·58	0·61	0·64	0·71			
	1·05	1·07	1·09	1·12	1·17	1·26			
	0·31	0·31	0·30	0·29	0·28	0·27	0·24		
8	0·49	0·50	0·51	0·52	0·54	0·57	0·63		
	0·91	0·92	0·94	0·95	0·98	1·02	1·10		
	0·28	0·28	0·28	0·27	0·26	0·25	0·24	0·22	
9	0·44	0·44	0·45	0·46	0·47	0·49	0·52	0·57	
	0·80	0·81	0·82	0·83	0·85	0·87	0·91	0·97	
	0·26	0·26	0·25	0·25	0·24	0·24	0·23	0·22	0·20
10	0·39	0·40	0·40	0·41	0·42	0·43	0·45	0·47	0·52
	0·72	0·72	0·73	0·74	0·75	0·76	0·78	0·81	0·88
	0·12								
25	0·16								
	0·28								
	0·06								
50	0·08								
	0·14								
	0·03								
100	0·04								
	0·07								

TABLE III

(*The three values of redshifts for any pair* (k^{-1}, n) *are respectively* z_s, z_b *and* z_c)

Core $p = k\rho$	Envelope $d\rho = n\,dp$									
	n 1/k	1/k	1/k	1/k	1/k	1/k	1/k	1/k	1/k	1/k
k^{-1}	−1	−0·9	−0·8	−0·7	−0·6	−0·5	−0·4	−0·3	−0·2	−0·1
	0·75	0·73	0·72	0·70	0·68	0·66	0·63	0·60	0·56	0·51
2	2·02	2·07	2·13	2·20	2·28	2·39	2·54	2·75	3·10	3·88
	4·90	5·00	5·11	5·24	5·41	5·62	5·91	6·32	7·00	8·52
	0·55	0·55	0·53	0·52	0·51	0·49	0·47	0·45	0·42	0·39
3	1·47	1·50	1·54	1·58	1·63	1·70	1·79	1·92	2·13	2·57
	3·12	3·17	3·24	3·31	3·40	3·51	3·66	3·87	4·22	4·97
	0·27	0·27	0·26	0·26	0·25	0·25	0·24	0·23	0·22	0·20
7	0·71	0·73	0·74	0·76	0·78	0·80	0·83	0·88	0·95	1·10
	1·26	1·28	1·30	1·32	1·35	1·38	1·42	1·48	1·58	1·77
	0·24	0·24	0·23	0·23	0·22	0·22	0·21	0·20	0·19	0·18
8	0·63	0·65	0·66	0·67	0·69	0·71	0·74	0·78	0·84	0·96
	1·10	1·11	1·13	1·15	1·17	1·20	1·23	1·28	1·36	1·52
	0·22	0·21	0·21	0·21	0·20	0·20	0·19	0·18	0·17	0·17
9	0·57	0·58	0·59	0·61	0·62	0·64	0·66	0·70	0·75	0·86
	0·97	0·99	1·00	1·02	1·04	1·06	1·09	1·13	1·20	1·33
	0·20	0·19	0·19	0·19	0·18	0·18	0·17	0·17	0·16	0·15
10	0·52	0·53	0·54	0·55	0·56	0·58	0·60	0·63	0·68	0·77
	0·88	0·89	0·90	0·91	0·93	0·95	0·98	1·01	1·07	1·19

These can be scaled once we know the mass M or the radius r_s of the model. Thus we have

$$M = u_s r_s, \quad \rho_c = \frac{3}{4\pi}\left(\frac{a_s u_s}{M}\right)^2. \tag{36}$$

Table II gives the values of z_c, z_b and z_s for $k^{-1} = 2(1)\,10$ with n taking values from 1 to $(k^{-1}-1)$ in steps of 1 and for $k^{-1} = 25, 50, 100$ with $n = 1$. For some values of k the range $n \approx k^{-1}$ was investigated in finer details by giving n values from $(k^{-1}-1)$ to $(k^{-1}-0{\cdot}1)$ in steps of 0·1. These results are reported in Table III.

4.2 *Discussion of results*

Certain general properties emerge from these numerical results which will be summarized below.

(i) For a given n as k increases (i.e. as the core equation of state ' stiffens ') the curve $v(u)$ rises more steeply in the core and falls more rapidly in the envelope. This is seen from Fig. 2 in which the curves are drawn for $n = 1$, $k^{-1} = 2(1)\,10$. Thus u_b and v_b increase with k. For example for $k^{-1} = 10$, $u_b = 0{\cdot}144$, $v_b = 0{\cdot}018$ whereas for $k^{-1} = 3$, $u_b = 0{\cdot}231$, $v_b = 0{\cdot}104$. Sharper fall in envelope would tend to decrease u_s with increasing k. But as the starting value in envelope (u_b) is higher for a larger k this effect may be masked. Thus for the above cases, $k^{-1} = 10$, $u_s = 0{\cdot}1851$ and $k^{-1} = 3$, $u_s = 0{\cdot}309$. Decrease in u_s with increasing k may be seen

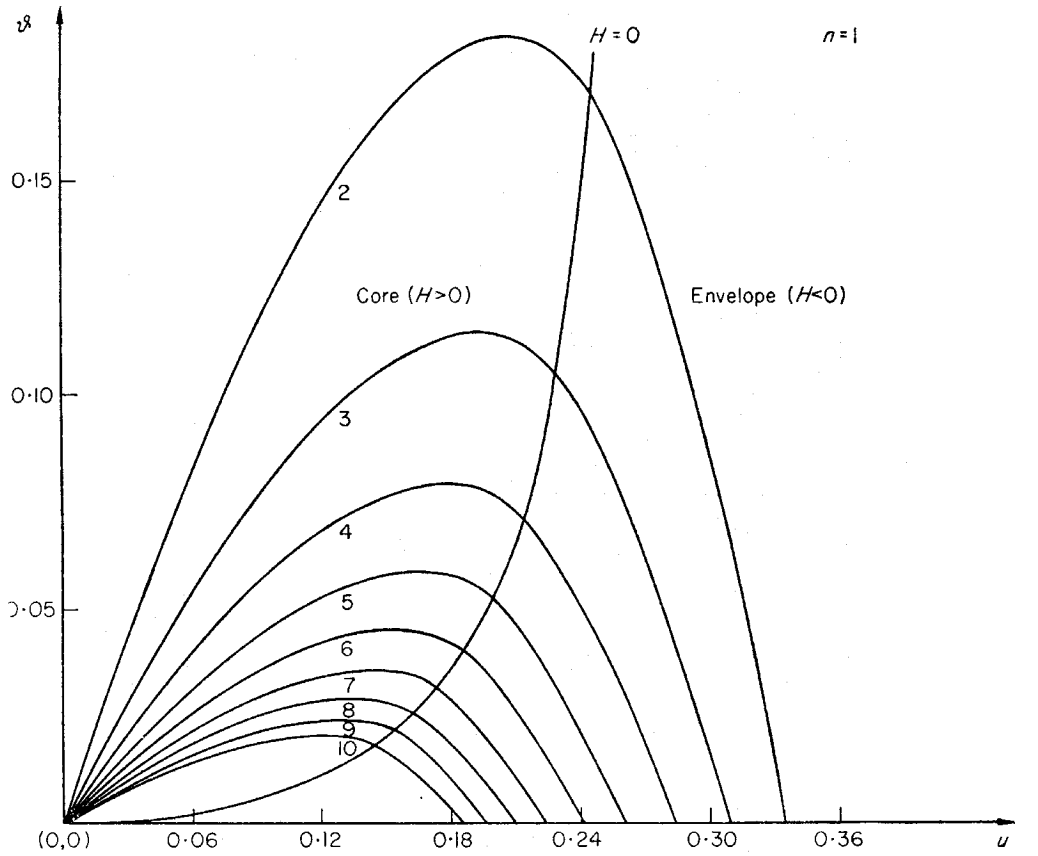

FIG. 2. *v(u) curves for different isothermal cores* ($\rho = k^{-1}p$) *with the same adiabatically stable envelope* ($dp = d\rho$). *The curves are labelled by the values of* k^{-1} *in the range* (2, 10).

by taking two close values of k. From this we expect a decrease in surface redshift z_s for a slight stiffening of equation of state in the core but an increase in z_s for a large stiffening. From (25) ,we see that the additional factor would tend to increase z_b as k increases. Whereas in (26), the factor p_c/p_b decreases with increasing k but the exponent $k/(k+1)$ increases. So behaviour of z_c would be more complicated. Summing up, we can say that for a large increase in k, all the three redshifts will increase. Thus for example, for $n = 1$, $k^{-1} = 10$, $z_s = 0{\cdot}26$, $z_b = 0{\cdot}39$ and $z_c = 0{\cdot}72$ while for $n = 1$, $k^{-1} = 2$ we have $z_s = 0{\cdot}75$, $z_b = 2{\cdot}02$ and $z_c = 4{\cdot}90$.

(ii) For a given k, as n increases, curves in Fig. 3 show that the $v(u)$ curves, which all start from the same point (u_b, v_b) become steeper and hence u_s decreases. For values of n close to k^{-1}, u as a function of v starts showing one or more turning points. For example, in the case $k^{-1} = 10$ the turning point appears when $n = 9$. However, in spite of the turning points the curves for different values of n do not seem to cross.

Decrease of u_s means a decrease of z_s as n increases. However, z_b and z_c increase. This is because the increase in the factors multiplying $(1+z_s)$ in (25) and (26), more than compensates the decrease in z_s. As $n \to k^{-1}$ this multiplying factor tends to infinity, whereas z_s stays positive. Thus z_b and $z_c \to \infty$ as $n \to k^{-1}$. It is not, however, possible to put $n = k^{-1}$. As pointed out by Bondi in I, this leads to an unbounded object.

Some of the trends exhibited by the numerical integrations can be deduced

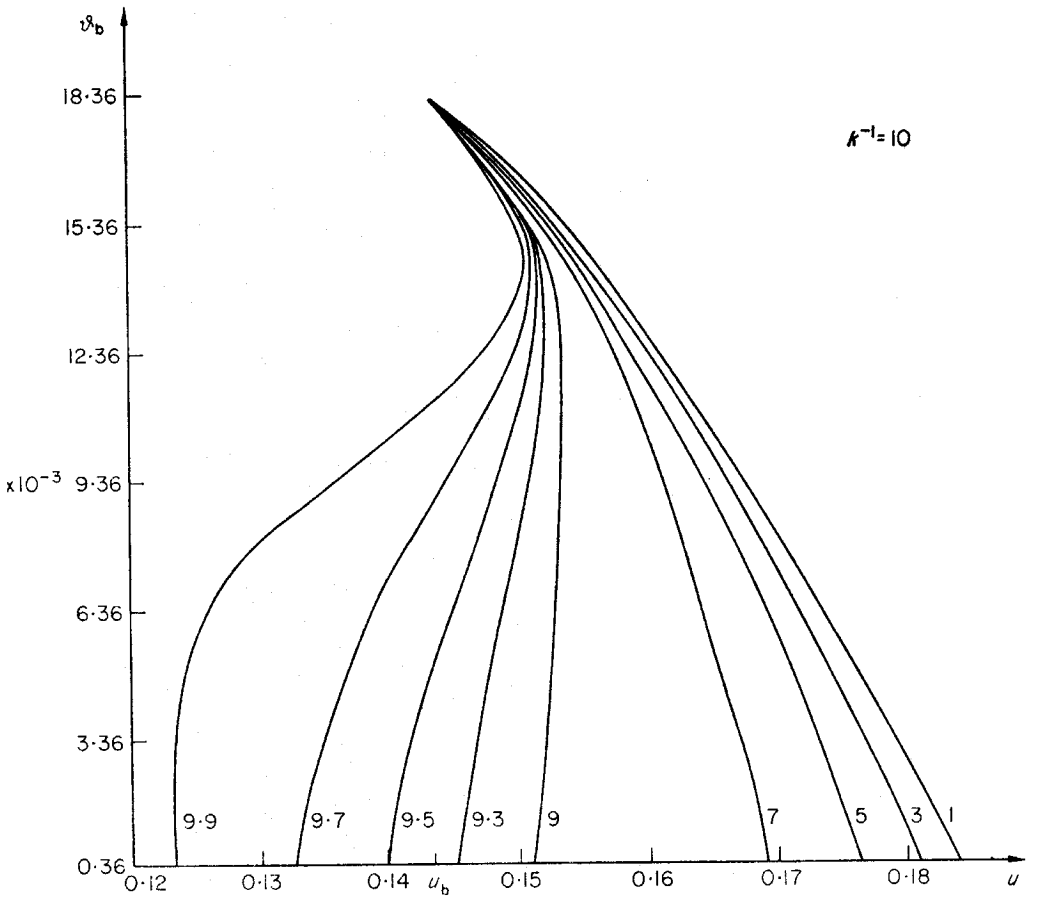

FIG. 3. *$v(u)$ curves representing different adiabatically stable envelopes ($d\rho = n\,dp$). The curves labelled by the values of n, start from the same point on $H = 0$. This is because they all have the same isothermal core given by $\rho = 10p$.*

analytically. For example we saw that u_b and v_b appear to increase with k. To deduce this we note that dv/du in the core increases with k so that for $k_2 > k_1$ the curve $v(u, k_2)$ always lies above the curve $v(u, k_1)$ in the core. Since these curves intersect the hyperbola $H = 0$ at points with coordinates $u < \frac{1}{4}$, $v < \frac{1}{4}$ (for the range of k-values considered) and v increases with u along the hyperbola $H = 0$ in the range $0 < u < \frac{1}{4}$, the result follows.

From the above discussions it is seen that even for small values of k (e.g. $k^{-1} \approx 10$ say) appreciable $z_c (\approx 1)$ can be obtained by taking n sufficiently large (e.g. $n \sim 9$). But as the rate of increase of z_c with respect to n is very slow, for very small k ($k^{-1} \approx 100$ say) appreciable z_c cannot be obtained unless n is very close to k^{-1}. Figs 4 and 5 show the variation of redshifts with k for fixed n and with n for fixed k, respectively. Summing up, the recipe for obtaining the highest central redshift appears to be: the ' stiffest ' possible equation of state in the core (i.e. the largest possible k) together with the most ' relaxed ' equation of state for the envelope (i.e. $n \to k^{-1}$ from below).

In general the equation of state in an actual object may be more complicated. However, over finite sections we can approximate it with the types of equations of state we have considered here. In this case the properties discussed above will provide qualitative guidance about the type of central redshift to be expected from the object.

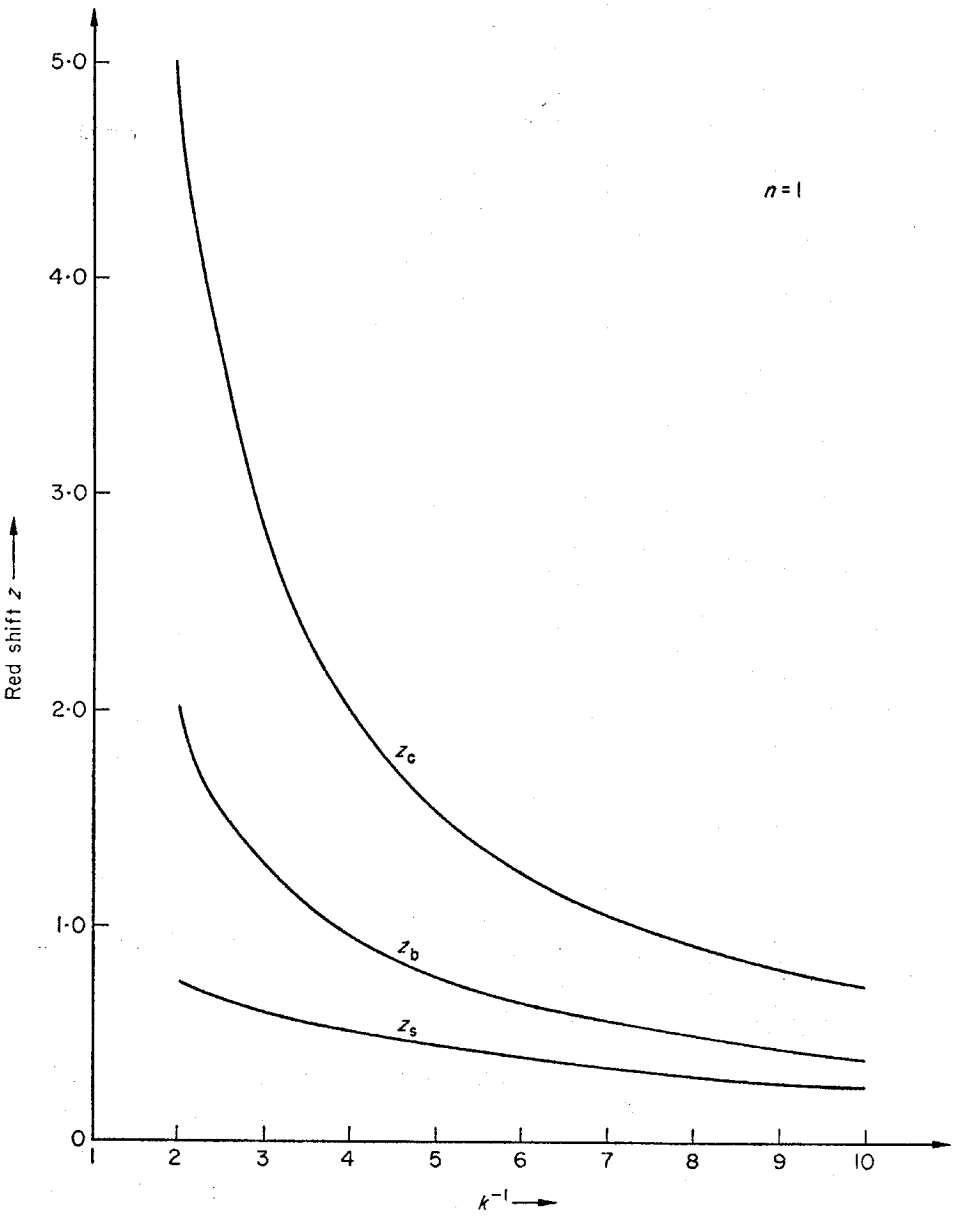

FIG. 4. *Curves showing the variation of surface, interfacial and central redshifts (z_s, z_b and z_c) with k^{-1} for a fixed n (=1). A typical point corresponds to an isothermal core ($\rho = k^{-1}p$) and an adiabatically stable envelope ($d\rho = dp$).*

5. LINE-WIDTH ANALYSIS

We now consider the above models in relation to QSOs and assume our object to consist of a finite, spherical, optically thin emitting region surrounded by a spherically symmetric distribution of a large number of compact highly-collapsed subunits. These provide the gravitational field and allow only a fraction β (<1) of the emission from the centre to escape. For the purpose of calculating the gravitational effects we will approximate the lumpy distribution in the exterior by the smooth distribution of the earlier sections.

We give below a version of the Greenstein–Schmidt calculation relating the mass of the object to the widths of emission lines coming from the centre rather than from the surface of the object. First we derive a general formula for the type

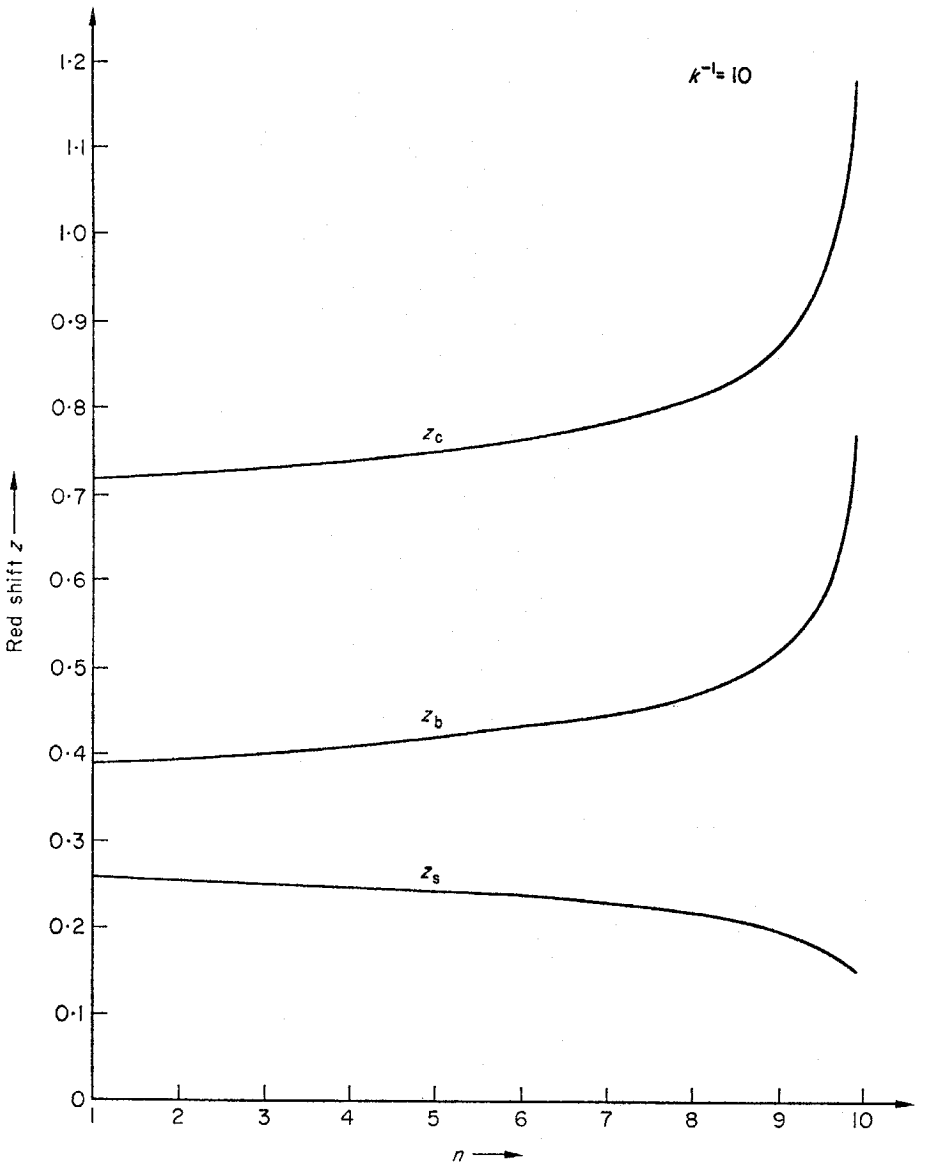

FIG. 5. *Curves showing the variation of surface, interfacial and central redshifts (z_s, z_b and z_c) with n for a fixed k^{-1} (= 10). A typical point corresponds to an isothermal core ($\rho = 10p$) and an adiabatically stable envelope ($d\rho = n\,dp$).*

of models discussed in Section 4. We then apply it specifically to the Lyman-alpha line because for $z > \sim 2{\cdot}3$, this line will be redshifted into the visible part. For illustration we shall use the data on 3C 9.

We assume that the observed width w of the emission line arises from the finite spherical emitting region at the centre. This line width arises from the variation of e^{ν} in the central region. As seen from Einstein's equations this variation is due to the variation of p and ρ in the emitting region. Since the lines are fairly narrow, the radius (in Schwarzschild coordinates) of this region is assumed to be small. We denote it by r_E and define

$$a_E = \sqrt{\frac{4\pi}{3}}\,\rho_c r_E. \tag{37}$$

Let λ and $\lambda+\Delta\lambda$ denote the emitted and observed wavelengths of the spectral line. We define another parameter

$$q = \frac{w}{\lambda+\Delta\lambda}. \tag{38}$$

Using (13) we get

$$\lambda+\Delta\lambda = \lambda \exp\{-\tfrac{1}{2}\nu(r_E)\}, \quad \lambda+\Delta\lambda+w = \lambda \exp\{-\tfrac{1}{2}\nu(0)\}. \tag{39}$$

This gives

$$1+q = \exp\tfrac{1}{2}\{\nu(r_E)-\nu(0)\} \cong 1+\tfrac{1}{2}\{\nu(r_E)-\nu(0)\}. \tag{40}$$

since near $r = 0$, ν is a slowly varying function and r_E is small. Near the origin we may use the approximations

$$u \approx \frac{4\pi}{3}\rho_c r^2, \quad v = 4\pi r^2 p_c$$

in the equation (8) to get

$$\nu(r_E)-\nu(0) \approx 4\pi r_E^2(k+\tfrac{1}{3})\rho_c. \tag{41}$$

Using (37), (40) and (41) we get

$$a_E^2 = \frac{2q}{(3k+1)}. \tag{42}$$

An identical expression is obtained by a more careful analysis using the power series expansion near the origin.

Let N_e be the average electron (or ion) density in the emitting region and α the constant giving the emissivity of the region as αN_e^2 (in erg cm^{-3} s^{-1}). Then the total flux in the spectral line is given by

$$L = \int_0^{r_E} 4\pi r^2 e^{\lambda/2}\alpha N_e^2\, dr,$$

$$\approx \frac{4\pi}{3} r_E^3 \alpha N_e^2 \tag{43}$$

since near the origin $e^{\lambda} \approx 1$.

If d is the assumed distance of the QSO and s the flux of radiation received from it in the given line we have

$$s = \frac{\beta L}{4\pi d^2(1+z_c)^2}. \tag{44}$$

In (44) we have assumed negligible cosmological component in the redshift so that $d \ll cH^{-1}$, H being Hubble's constant. The $(1+z_c)^2$ factor in the denominator on the right-hand side represents the combined effect of gravitational time dilation and photon energy degradation. Using (36), (37), (42), (43) and (44) we finally arrive at the following formula:

$$M = \frac{c^2}{G} a_s u_s \left\{\frac{(3k+1)}{2q}\right\}^{1/2}\left\{\frac{3s(1+z_c)^2}{\alpha\beta}\right\}^{1/3} N_e^{-2/3} d^{2/3}. \tag{45}$$

The factor c^2/G has crept into the coefficient on the right-hand side of (45) because we now wish to express M in cgs units.

In applying (45) to actual observations, we must remember that s, z_c and q are supplied by observations. a_s, u_s and k are determined by the model which produces the required z_c. α and N_e must depend on the astrophysical considerations of the emitting region. c and G are physical constants. Thus we may look upon (45) as a relation between M and d when all other quantities have been specified.

To illustrate this we take the example of the QSO 3C 9. Using the following data (7):

$$z = 2{\cdot}012, \quad w = 460 \text{ Å}, \quad s = 1{\cdot}154 \times 10^{-13} \text{ erg s}^{-1} \text{ cm}^{-2} \tag{46}$$

and choosing $k^{-1} = 4$, $n = 2$ (which gives $z_c \simeq 2{\cdot}0827$), $a_s = 1{\cdot}5295$, $u_s = 0{\cdot}2754$, we get

$$\frac{M}{M_\odot} = 2{\cdot}327 \times 10^7 \beta^{-1/3} \alpha^{-1/3} N_e^{-2/3} d_{\text{mpc}}^{2/3} \tag{47}$$

where d_{mpc} is the distance expressed in megaparsecs. For Lyman alpha, $\alpha \approx 10^{-22}$, $N_e \approx 10^8$ do not seem unreasonable. This gives for $\beta \approx 0{\cdot}5$

$$M \approx 5 \times 10^{10} M_\odot \tag{48}$$

for a distance $d_{\text{mpc}} \approx 100$. That is, we require the QSO to have mass of the order of that of a galaxy, for a distance small enough for the cosmological redshift to be negligible. It is interesting to note that the ratio of the mass of the emitting region to the total mass is 0·129, so that the emitting region would have a mass

$$\sim 6{\cdot}45 \times 10^9 M_\odot.$$

Clearly, these calculations rule out the possibility of the QSO being a starlike object in the Galaxy. For, if we use the rule adopted in (4) that the QSO should not exert a gravitational field exceeding 10 per cent of that of the Galaxy in our neighbourhood, we have

$$\frac{M}{M_\odot} \leqslant 10^{14} d_{\text{mpc}}^2. \tag{49}$$

If we set $d_{\text{mpc}} = 0{\cdot}01$ (i.e. $d = 10$ kpc), we get $M \leqslant 10^{10} M_\odot$. Scaling down (48), however, we get for this distance $M \approx 10^8 M_\odot$. Thus although (49) is satisfied, we still end up with a mass considerably in excess of stellar masses.

We emphasize here the model dependent aspect of this calculation as well as that in (4). In estimating α and N_e it is usual to draw upon the experience of other astronomical objects. In (4) for example the guidelines were set by gaseous nebulae and young stars in the solar neighbourhood with an estimated electron temperature $T_e \sim 16\,800$ K. Whether the same physical conditions operate in the centres of such highly redshifted objects as 3C 9 (assuming the redshift to be gravitational) is open to question. Also, in (47) a higher N_e will reduce $M/M_\odot$. In (4) an upper limit was set on N_e by the appearance of forbidden line [O III] λ 5007 in the spectra. This line does not appear in the spectrum of 3C 9, because of its high redshift. Does this mean we can assume it is not present and adopt higher values of N_e?

We mention these queries to point out that the mass estimates in the line width analysis are based on a number of assumptions which are open to question. Even taking these for granted, the mass estimate (48) is not enormously high but is quite reasonable, provided we consider QSOs as extragalactic objects.

6. CONCLUDING REMARKS

To summarize, it seems possible to construct models of massive objects in equilibrium giving high central redshifts without making undue demands on the equation of state. Although we have taken a spherically symmetric system to simplify computations, in practice we expect the object to be filled with small dense subunits interspersed with absorbing clouds so that the emission from the centre can get out. The line width analysis then tells us that such objects may be of galactic masses if their distances do not exceed 100 mpc.

According to this point of view the QSO redshift z consists of two components: the cosmological component $z_{\rm cos}$ and the gravitational component $z_{\rm grav}$, so that

$$(1+z) = (1+z_{\rm cos})(1+z_{\rm grav}). \tag{50}$$

We expect $z_{\rm cos}$ to be small, in any case of the same order as galactic redshifts so far known. Thus for $z \approx 3{\cdot}5$, $z_{\rm cos} \approx 0{\cdot}2$, we require $z_{\rm grav} \approx 2{\cdot}75$. We do not wish to enter here into arguments why an intrinsic component cannot be ruled out at present. This discussion has appeared extensively in literature (*cf.* (1)). We only point out that gravitational reshift can account for a substantial part, if not whole, of a QSO redshift.

In conclusion we wish to argue that a Parkinsonian situation exists in astronomy. Black holes with their infinite redshifts have been readily accepted by the astronomical community; yet the same community appears to have a prejudice against objects having gravitational redshifts of the order of 2 or 3!

ACKNOWLEDGMENTS

We thank Professor W. A. Fowler for making available to us some of his unpublished work on gravitational redshifts in models based on the Schwarzschild interior solution. We also thank Mr R. K. Chopra for assistance with numerical computations. One of us (JVN) acknowledges the award of a Jawaharlal Nehru Fellowship.

REFERENCES

(1) Burbidge, G. R., 1973. *Nature*, **246**, 17.
(2) Hazard, C., Jauncey, D. L., Sargent, W. L. W., Baldwin, J. A. & Wampler, E. J., 1973. *Nature*, **246**, 205.
(3) Wampler, E. J., Baldwin, J. A., Burke, W. L., Robinson, L. B. & Hazard, C., 1973. *Nature*, **246**, 203.
(4) Greenstein, J. L. & Schmidt, M., 1964. *Astrophys. J.*, **140**, 1.
(5) Bondi, H., 1964. *Proc. R. Soc. A*, **282**, 303.
(6) Hoyle, F. & Fowler, W. A., 1967. *Nature*, **213**, 373.
(7) Oke, J. B., Neugebauer, G. & Becklin, E. E., 1970. *Astrophys. J.*, **159**, 341.